Diamond & Related Materials 82 (2018) 63–69

Contents lists available at ScienceDirect

Diamond & Related Materials

journal homepage: www.elsevier.com/locate/diamond

Synthesis of MoC@Graphite NPs by short and ultra-short pulses laser ablation in toluene under N_2 atmosphere

Madelyn Madrigal-Camacho[a,b,*], Alfredo Rafael Vilchis-Nestor[b,*], Marco Camacho-López[c], Miguel A. Camacho-López[d]

[a] Posgrado en Ciencia de Materiales Faculty of Chemistry, UAEM, Toluca, Mexico
[b] Centro Conjunto de Investigación en Química Sustentable UAEM-UNAM, Km 14.5 Toluca-Atlacomulco Road, Campus Rosedal, Toluca, CP 50200, Mexico
[c] Laboratorio de Investigación y Desarrollo de Materiales Avanzados, Facultad de Química, UAEM, Campus Rosedal, Km 14.5 Toluca-Atlacomulco Road, Toluca C.P. 50295, Mexico
[d] Laboratorio de Fotomedicina, Biofotónica y Espectroscopía Láser de Pulsos Ultracortos, Facultad de Medicina, UAEM, Jesús Carranza y Paseo Tollocan s/n, Toluca C.P. 50180, Mexico

ARTICLE INFO

Keywords:
Laser ablation
Short and ultrashort pulses
Molybdenum carbide nanoparticles
Onion-like carbon nanostructures

ABSTRACT

In this work, we present the experimental methods of the synthesis of MoC/MoC@Graphite by laser ablation with short and ultra-short laser pulses by using a molybdenum (Mo) and graphite target. All the experiments were carried out utilizing toluene as liquid medium. During the ablation, a nitrogen (N_2) atmosphere was necessary to avoid the oxidation of the Mo NPs. The structure, composition, and morphology of the NPs were investigated by transmission electron microscopy (TEM-HRTEM-SAED), X-ray diffraction and Raman spectroscopy. The TEM results evidence the formation of two carbonaceous structures: a graphite coating around the NPs and an amorphous carbon matrix that embeds the NPs. It was observed that these structures contribute to avoid the agglomeration and oxidation of the NPs. The size distribution, structure, and agglomeration of the NPs were discussed based on the solvents and also on the duration of the laser pulses.

1. Introduction

Laser ablation of Solids in Liquids (LASL) is one of the most efficient techniques in the synthesis of NPs which is characterized by being relatively simple due to long reaction times, high temperatures or multi-step chemical synthesis procedures not being required [1–3]. The main formation mechanism consists in nucleation during the plasma plume cooling and then, followed by growth and coalescence of NPs [4]. The colloidal solutions produced are stable without adding stabilizing surfactants or ligands and also hazardous or toxic chemical precursors [5] which lead to the generation of pure NPs without residual contaminants and therefore not chemical waste is generated thus contributing to the environment.

Based on the nature of the material, the NPs synthesized may show inhomogeneous particle sizes, agglomeration, and oxidation. One of the ways to avoid these problems is to functionalize the bare NPs by adding a ligand or a surfactant into the colloidal solution just after being synthesized or during the ablation [6–8]. Nevertheless, in this case, the encapsulation of NPs has been developed to form core-shell structures, with the specific aim to avoid the oxidation of the molybdenum.

In order to avoid the oxidation of molybdenum, a carbon coating is a viable and efficient option. The alternative to form this coating is by the laser ablation of a hydrocarbon liquid. It has been reported that laser ablation allows the formation of Onion-like Carbon (OLC) as a coating of the carbide. Currently, these structures are one of the most interesting nanoforms among all the carbon allotropes due to its electrical conductivity, high specific surface area, tribological and catalytic properties, electrochemical energy storage and a high potential in biomedical applications [9–11].

Carbon coating is produced by the effect of the high temperature of the plasma plume which induces a thermochemical decomposition (pyrolysis) of the liquid thus causing the carbon particles generation [5,12,13]. The saturated carbon particles will precipitate and grow as a carbon coating around the NPs during the following rapid quenching process of the laser ablation. The nature of the organic solvent used affects the coating (forming either an amorphous or graphitic coating), and the growth, features, stability, chemical composition and size/morphology of the NPs (some cases are presented in several papers) [14–17].

On the other hand, the synthesis of carbides NPs, specifically

* Corresponding authors at: Centro Conjunto de Investigación en Química Sustentable UAEM-UNAM, Km 14.5 Toluca-Atlacomulco Road, Campus Rosedal, Toluca, CP 50200, Mexico.
E-mail addresses: mmadrigalc249@alumno.uaemex.com (M. Madrigal-Camacho), arvilchisn@uaemex.mx (A.R. Vilchis-Nestor).

https://doi.org/10.1016/j.diamond.2017.12.019
Received 19 October 2017; Received in revised form 7 December 2017; Accepted 27 December 2017
Available online 28 December 2017
0925-9635/

molybdenum carbide by LASL has not been extensively studied [18]. However, the interest in studying this carbide has recently grown due to its catalytic properties (similar to noble metals in many organic chemical reactions) [19–22]. Besides, it is a carbide with a great number of stable phases [23] with a high thermal stability and oxidation resistance [24].

Considering the impact of laser ablation on NPs synthesis and various properties (chemicals, physical, and mechanics) of molybdenum carbide, the present work focuses on the combined implementation of three strategies. Firstly, the experiments were carried out using short ablation time with low energy, thus decreasing the energy cost required for the synthesis of the NPs. Secondly, mitigates the oxidation of the molybdenum by the presence of N_2 atmosphere and by the graphitic coating around the NPs, since Mo is oxidized in organic solvents in O_2 atmosphere using the same ablation parameters. Besides, under oxidizing atmosphere OLC structures were not observed for molybdenum carbide [18,25]. Finally, beyond the synthesis tests, this work also aims to improve the knowledge of the role of the pulse duration in laser ablation regarding size distribution, the morphology of NPs and the formation of a graphitic coating.

2. Experimental

2.1. Laser ablation of Mo and graphite in N_2 atmosphere

The colloidal suspensions were synthesized by using a molybdenum and graphite target (disks with thickness of 3 mm and 3.7 mm respectively, 99.9% purity, Kurt J. Lesker Co.) in toluene (as liquid medium) under a nitrogen atmosphere. The experimental setup used in the laser ablation experiments is shown in Fig. 1.

The experiments were performed by using two different Nd:YAG lasers of short and ultra-short pulses, both with a wavelength of 1064 nm and a repetition rate of 10 Hz. One of them is a nanosecond laser: Surelite Cotinuum (short pulses, $\tau \sim 6$ ns) and the other one is a picosecond laser: Ekspla (ultra-short pulses, $\tau \sim 30$ ps). The incidence angle of the laser beam respect to the normal line of the target was 45° (see Fig. 1).

Firstly, the Carbon NPs were produced by irradiating the graphite for 3 min, using a per pulse laser energy of 25 mJ, which corresponds to a per pulse laser fluence of 3.68 J/cm^2 for ns laser and 0.79 J/cm^2 for ps laser. Finally, the molybdenum target was ablated for 5 min with a per pulse laser energy of 50 mJ, corresponding to a per pulse laser fluence of 7.36 J/cm^2 for ns laser and 1.6 J/cm^2 for ps laser. The NPs suspension was sonicated each minute in order to disperse those precipitated NPs, besides the vapors generated by toluene were removed by inserting a needle into the septum stopper.

2.2. Characterization of samples

The produced NPs were analyzed by TEM (JEOL-2100 with 200 kV acceleration voltage and LaB_6 filament) in order to determine the size distribution, morphology, structure and chemical composition of the NPs and the carbonaceous structures. The sample was prepared firstly by dispersing the NPs in ethanol to eliminate the organic residual components and then the solution was dropped onto a carbon-coated copper grid.

At least 5 representative images were taken for each sample. In order to obtain statistically consistent information. Particle size distributions were obtained by the measurement of more than 100 particles for each sample, employing ImageJ™ software. The average particle size diameters were calculated with the equation $d_{avg} = \Sigma(n_i d_i) / \Sigma n_i$ where n_i is the number of particles of diameter d_i. It is important to mention that HRTEM analysis was performed with DigitalMicrograph™ (DM) software provide by Gatan Microscopy.

To analyze the graphite coating of NPs and the matrix of amorphous carbon formed, microRaman spectroscopy was utilized. The collected powder of NPs (previously washed with ethanol and dried at room temperature) was characterized using a micro-Raman system (LabRamam HR-800 of Jobin-Yvon-Horiba) with a 632.8 nm He-Ne laser as excitation source. To conclude, X-ray diffraction (XRD) was performed to obtain the structural composition of laser ablated NPs. A Bruker D8 Advance system with CuKα radiation and Lynxeye detector ($\lambda = 0.15419$ nm, scan step size of 0.03° and time per step of 114 s) was used.

3. Results and discussion

3.1. Laser ablation of Mo in toluene with N_2 atmosphere by using ns laser pulses

All the experiments presented here were carried out in toluene, using a closed system with N_2 atmosphere. It has been proved that using toluene as the liquid medium in the LASL technique carbides NPs and graphite coatings can be obtained. The extreme conditions of high temperature and high pressure of the plasma plume allows the decomposition of the solvent forming ions, radicals, and atoms of Carbon that can combine with the species of metals in the plasma plume [13,26].

The production of the NPs with the N_2 atmosphere system was attempted with both short and ultra-short pulses with the purpose of

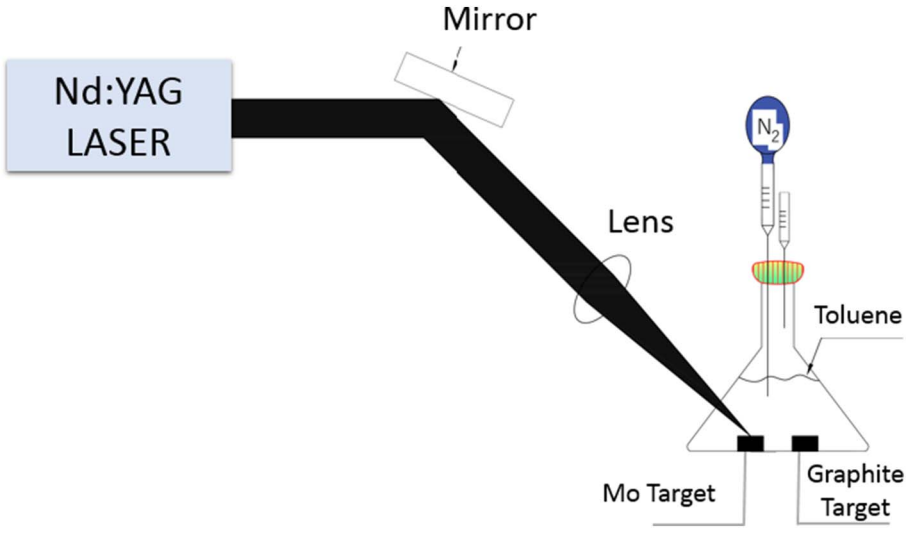

Fig. 1. Experimental setup for the laser ablation experiments in N_2 atmosphere.

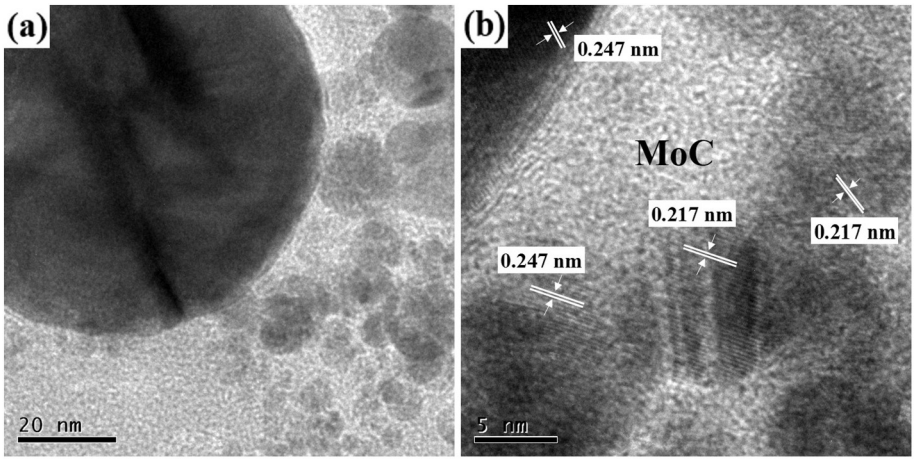

Fig. 2. TEM micrograph (a) and HRTEM image (b) of NPs obtained by laser ablation of a Mo target in toluene in N_2 atmosphere. JCPDS card No. 03-065-8092.

comparing both systems. The size distribution, morphology and the formation of graphite coating around the NPs were analyzed by TEM.

With the purpose of corroborating that the closed system works properly, avoiding the oxidation of the NPs and achieving the synthesis of the molybdenum carbide NPs with the graphitic coating, a synthesis of Mo target by short pulse laser ablation ($\tau \sim 6$ ns) in toluene was carried out.

Fig. 2a reveals spherical NPs with a non-homogeneous size distribution. The HRTEM micrographs in Fig. 2b shows clearly lattice fringes of (111) and (200), with an interplanar spacing of 0.247 nm and 0.217 nm, corresponding to the cubic phase of molybdenum carbide δ-MoC (JCPDS card No. 03-065-8092). The formation mechanism of the carbide could be possible due to the toluene decomposition. The high excitation energies inside the plasma plume allow the pyrolysis of the toluene [13] that causes the formation of C species. Consequently, as a result of chemicals reactions, complexes of carbon and molybdenum can be formed [25]. The nucleation and growth of the MoC NPs are performed inside the cavitation bubble. Finally, in the stage of plasma cooling, the MoC NPs are ejected and stabilized with the surrounding liquid.

With this method, the graphite coating was not observed, which means that the number of carbon particles only reacted with the Mo NPs to form the molybdenum carbides NPs, but no graphitization process has been observed by this technique. In order to improve the encapsulation, the NPs with graphite, carbon NPs were added due to the carbon supplied by the toluene was not enough to obtain a homogenous coating. To achieve that goal, an additional laser ablation step was performed on a graphite target before the ablation of the Mo target.

During this step spherical C NPs and OLC structures were obtained (Fig. 3 a–b). The exhibited crystal fringes in Fig. 3b was the (100) plane of graphite with the d-spacing of 2.09 nm, (JCPDS card No.75-2078). It was observed that some of the C NPs were coated by graphitic layers with a thickness between 3 and 5 nm, the distance of each layer is 0.34 nm. On the other hand, some of the C NPs obtained are embedded in an amorphous carbon matrix as well. In Fig. 3c the Raman spectrum clearly shows the D-band at 1370 cm^{-1} which is associated with the crystalline disorder and structural defects of the graphite [27], while G band at 1590 cm^{-1} corresponds to the crystallinity of graphite [28]. The D-band was more intense and broader compared with G-band, demonstrating that the material possesses low crystallinity. There is a possibility that the amorphous carbon, which embeds the NPs, intervenes in the detection of the high intensity of the D-band.

3.2. Laser ablation of MoC and MoC@Graphite core-shell NPs by using ps laser pulses with N_2 atmosphere

Fig. 4a shows the size distribution of the NPs obtained by ultra-short pulse laser ablation, which is smaller compared with the previous method discussed in Section 3.1. The particle morphology was also spherical with an average size of 5.96 ± 3.7 nm. NPs obtained in this experiment are embedded in an amorphous carbon matrix, it can be assumed that this matrix is not only responsible for control of morphology and size, but also prevents agglomeration of the NPs. Moreover, in Fig. 4b is evident that the NPs are also encapsulated in a graphitic carbon structure, the so-called onion-like carbon structures (OLC) [29–32]. The distance between each carbon-layer is 0.34 nm (Fig. 3b), which can be associated with graphitic layers range (0.335 nm) [33]. The minimum variation of the experimental layer distance in contrast

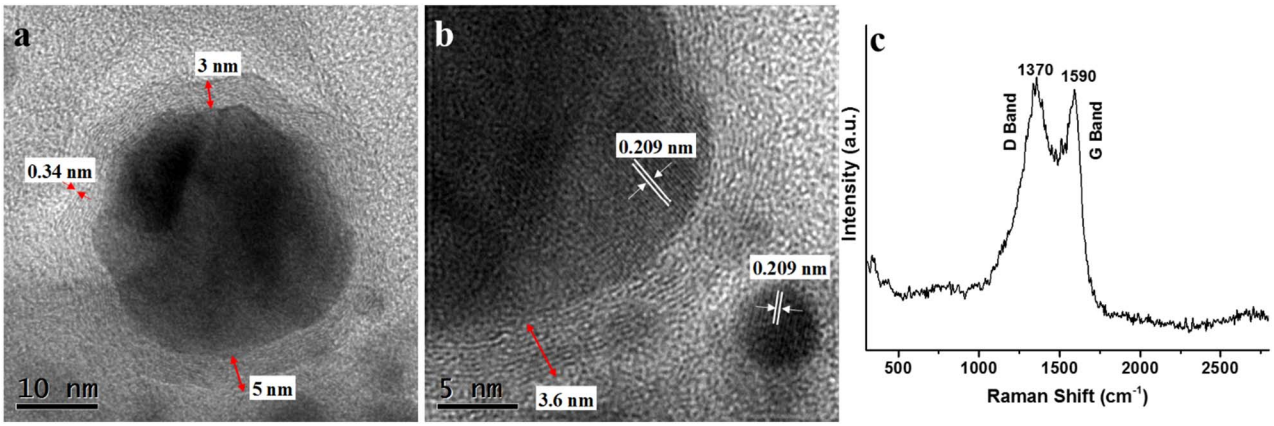

Fig. 3. (a) TEM and (b) HRTEM micrographs of C NPs and OLC structures obtained by laser ablation of a graphite target in toluene. (c) Raman spectrum of carbon nanostructures. JCPDS: 75-2078.

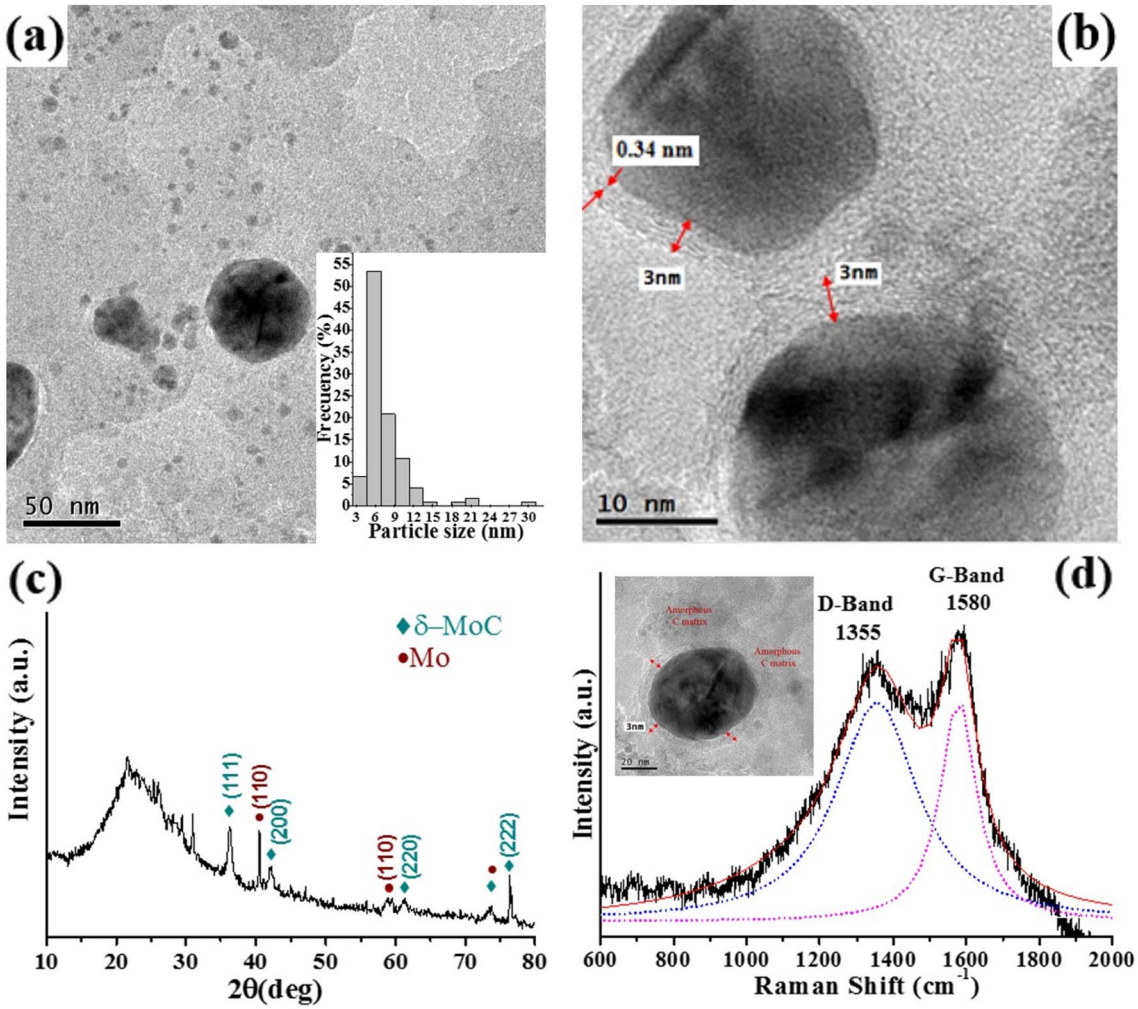

Fig. 4. (a) TEM micrograph of the NPs ablated in toluene under N_2 atmosphere. Inset: histogram of size distribution, (b) HRTEM image for MoC@Graphite, (c) XRD patterns of NPs and (d) Raman spectrum (the dashed lines represent the deconvolution in two Lorentzian curves (and its sum) corresponding to the D and G bands) JCPDS cards No.03-065-8092 and No. 03-065-8092.

with theoretical one may be due to the strain between the planes in order to minimize the superficial energy of the semi-spherical particle. The average thickness of layers is 3 nm, which remains fairly stable for large and small NPs.

Fig. 4c shows XRD patterns of MoC NPs generated by ultra-short pulse. The Bragg reflections reveal that there are crystalline particles but it also exists amorphous material. The peaks were assigned to diffraction from the (111), (200), (220) and (222) planes of face-centered cubic (FCC) structure (JCPDS card No. 03-065-8092) with a lattice parameter of a = 4.28 Å. Furthermore, the XRD pattern (Fig. 4c) confirms that the carbide formation was not completely formed in the solution, due to the presence of elemental Mo, so an inhomogeneous mixture of δ-MoC, Mo, and amorphous carbon was obtained (broad peak between 15° and 30° corresponds to amorphous C).

The oxidation of Mo was successfully avoided; this is confirmed by microRaman spectrum reported in Fig. 4d. It is well known that molybdenum oxides present Raman signals in the range 100–1100 cm^{-1} [34–37], being the more intense from 600 to 1100 cm^{-1}. As one can see from Fig. 4d no Raman signals are present in the range from 300 to 1100 cm^{-1}, indicating that molybdenum oxides are not formed during the ablation process. Carbon coating around the NPs fulfills the function of protecting them from the oxidation after the synthesis and the N_2 atmosphere during the ablation. The Raman spectrum is dominated by the amorphous carbon signals, with the D band at 1355 cm^{-1} and G band at 1580 cm^{-1}. There is a probability that the bands of amorphous carbon are overlapping with OLC signals or also the OLC signals definitely cannot be detected due to the amorphous carbon encapsulates the graphitic structure with a high thickness (see micrograph inset the Fig. 4d).

3.3. Formation process of MoC-graphite core/shell NPs

Two different carbon structures have been obtained, graphite coating around the NPs and amorphous carbon matrix which embeds the NPs. It is evident that the graphite layers have defects probably because of the disordered layers at the edges and the addition of H atoms and remnant O_2 molecules from the toluene into the graphite layers, probably these are two of the causes that carbon cannot crystallize.

To better understand the formation process of the two carbon structures it is necessary to consider the laser ablation mechanism. The high temperature and pressure of the plasma plume induce the ionization of the toluene, thereby generating ions and/or atoms of C and H and some radicals which can react with Mo species (atoms, ions, clusters, etc.) during the nucleation process and during the adiabatic expansion of the plasma plume. As a result, MoC is formed from the chemical reactions due to the high concentration of carbon species from the solvent.

Nevertheless, as mentioned above the carbon from the toluene was not enough to form the graphite coating around the MoC NPs. Outside

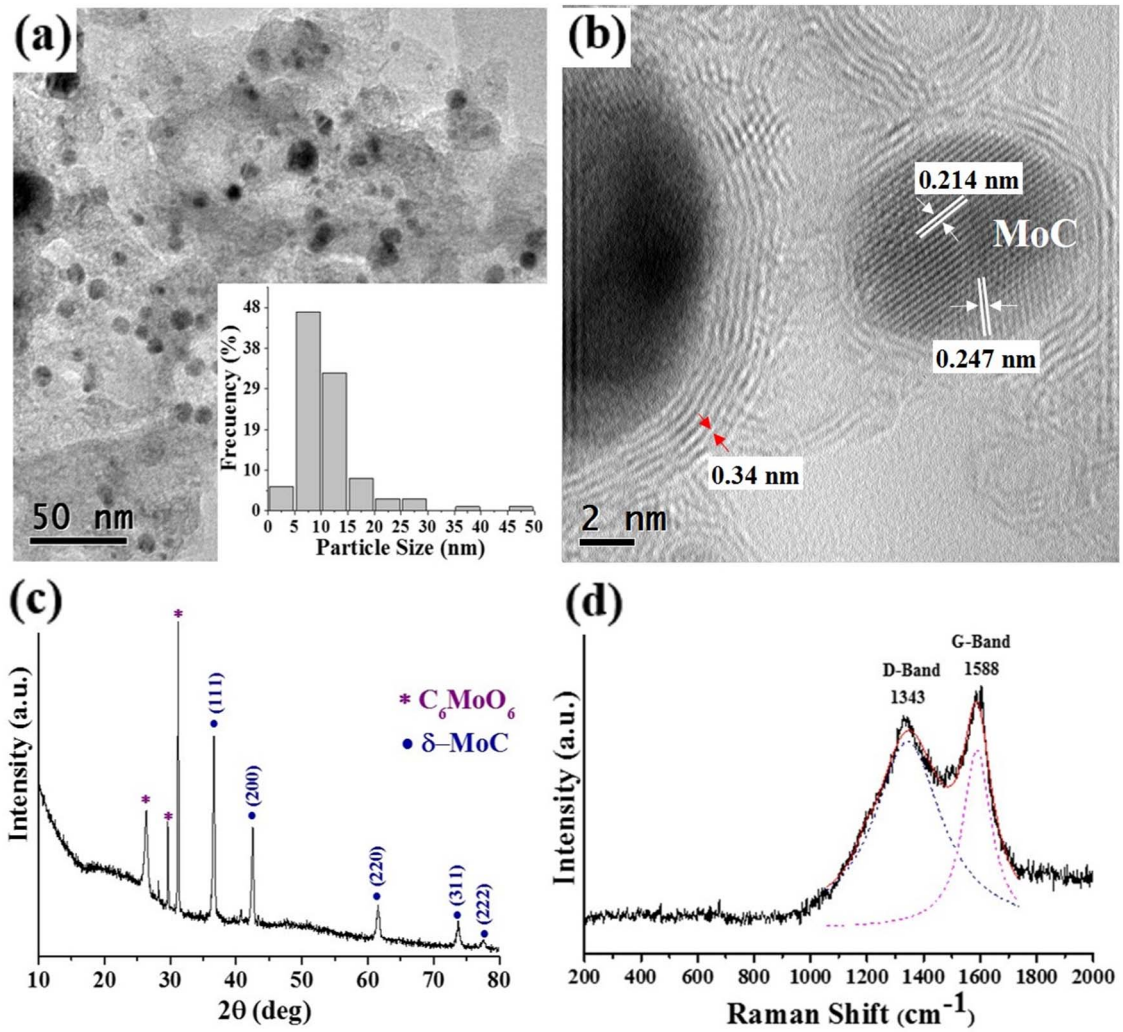

Fig. 5. (a) TEM micrograph of the NPs ablated in toluene under N_2 atmosphere. Inset: histogram of size distribution, (b) HRTEM image for amorphous carbon matrix and OLC coating of the enlarged area of NPs, (c) XRD patterns of NPs and (d) Raman spectrum (the dashed lines represent the deconvolution in two Lorentzian curves (and its sum) corresponding to the D and G bands). JCPDS cards No. 03-065-8092 and No. 00-012-0691.

the cavitation bubble, C NPs from the ablation of the graphite target precipitates on the NPs surface into a MoC/graphite core-shell NPs due a rapid cooling process.

During the plasma cooling down the NPs are rapidly quenched, allowing not all the carbon reacts to form the graphite coating. The excess carbon is saturated on the core/shell NPs in an amorphous carbon matrix. Consequently, the NPs are ejected and transferred into the solvent which will be subsequently exposed to continuous irradiation by the pulsed laser causing more amorphous carbon can condense on the particles surface. It was observed that the duration of the pulse has an important role in the formation and thickness of the carbon coatings, thus causing important effects on the size of the NPs.

3.4. Laser ablation of MoC and MoC@Graphite core-shell NPs by using ns laser pulses with N_2 atmosphere

In order to further confirm the effect of the pulse duration on the formation of the graphite/amorphous coating and size of the NPs, we performed laser ablation experiments with ns laser pulses. With short pulses, a greater number of NPs were obtained and these showed a higher particle size distribution (Fig. 5a) comparing to the NPs obtained with ultra-short pulses. The micrograph in Fig. 5a clearly illustrates the spherical morphology of the NPs formed. The inset in Fig. 5a shows the histogram of size distribution of NPs obtained with short pulse laser ablation. The average particle size is 11.07 ± 6.66 nm, which confirm that longer pulses produce larger particles.

Fig. 5b shows more clearly the graphitic coating around the NPs. With this system, more OLC structures were obtained and the number of layers is less uniform around the NPs and also a disorder of the layers can be observed when the NPs are connected to other NPs. The crystal fringes were the (111) and (200) planes of cubic MoC with the d-spacing of 0.214 and 0.247 nm respectively (JCPDS card No. 03-065-8092).

In this experiment, the amorphous carbon was predominant due to more carbon species were formed from the decomposition of toluene. This can be explain based on the fact that longer pulses have a higher laser energy fluence threshold and also deliver more energy to the target and solvent comparing with ultra-short pulses. With ns pulses, the laser-matter interaction coexists for a longer time and more energy is transferred to the plasma plume with a consequent increase in its temperature, pressure and lifetime [38–40] which causes more carbon species are formed from the ionization of the toluene and consequently those C particles quick reach a supersaturate condition and finally form the amorphous matrix.

Another explanation of the formation of more amorphous carbon in the ns ablation is due to a higher absorption by the already formed MoC and MoC@graphite NPs. These NPs could react with other C NPs, causing more carbon to be adhered to the surface, but these C structures

are not able to crystallize as graphite coating since the quenching is not cold enough by the remnants thermal effects which imply only amorphous structures can be formed.

With XRD and Raman analysis were not possible to obtain signals of graphite since amorphous carbon predominates in the system, which must mask the signals of graphitic structures. Fig. 5c shows δ-MoC as the predominant phase with no presence of elemental Mo. The formation of C_6MoO_6 is attributed to residual oxygen molecules inside the system since anhydrous toluene was not used, or due to a post-reaction when the system was opened to O_2 atmosphere at the end of the laser ablation, which indicates the carbon coating not stabilizes the NPs completely, but enough to prevent the oxidation of the NPs in O_2 atmosphere. Besides that, there is not a specific change in Raman spectra, only D band is broader and presents a downshift due to the increase in structure defects (Fig. 5d).

The pulse duration plays an important role in the size distribution of NPs. This work has shown ns pulses produce NPs with a larger size than ps pulses. It has been explained through the thermal effect during the ablation where the surface of the target heats due to the absorbed energy, which leads to melting and vaporization, thereby causing the release of larger particles due to the explosive boiling effects due to the short relaxation times between pulses [41–42] and also, it is due to the interaction of cavitation bubbles (CB) [43]. With ns pulses, CB are larger and have a longer lifetime encouraging more nucleation processes and greater particle growth [44].

In addition, another possible explanation is that the ablation efficiency is lower in the synthesis by ultra-short pulses compared with short pulses, thus generating the particles are smaller in the ps pulsed laser. This is reflected in the size distribution of NPs obtained in both systems (Figs. 4a–5a).

4. Conclusions

We have investigated an alternative to synthesis MoC NPs in order to avoid the oxidation of Mo NPs during laser ablation in toluene. δ-MoC was obtained using a closed system with N_2 atmosphere in toluene and no presence of oxides was observed. The results suggest that the carbon particles from the toluene decomposition participated directly in the synthesis of carbide. Besides, C NPs from the ablation of the graphite target promote the formation of the graphite coating and amorphous carbon matrix. Significantly difference in the carbon structures was obtained by short and ultra-short laser ablation. HRTEM results have shown that using ns laser pulses the amorphous carbon matrix predominates and embeds the NPs. In the case of the ablation with ps laser pulses, the amorphous carbon matrix was detected with less thickness which allowed a better analysis of the graphite coatings. However, the number of OLC structures in both systems did not represent the majority of the structures formed. It is a fact that the pulse duration of the applied laser source affects the size distribution and morphology of the NPs and the carbon coating reduces the agglomeration of the NPs. The procedure reported could be easily applied to fabricate carbides-graphite core-shell NPs of other metals in order to prevent its oxidation. However, to improve the graphite coating, more studies are required about the influence of important parameters like the time of the irradiation of the graphite target and the energy fluence of the laser to ablate the metal in presence of C NPs in toluene, during the OLC formation.

Acknowledgements

This work was supported by CONACYT (Grant No. 280518) and UAEM (Grant Number 1025/2014RIFC). We also thank Dr. Uvaldo Hernández from CCIQS for technical assistance in DRX. The author Madrigal-Camacho thanks to CONACYT for the Grant No. 708628.

References

[1] N. Semaltianos, Nanoparticles by laser ablation. Solid state and materials, Sciences (2010) 105–124.
[2] F. Mafuné, K. Miyajima, Sobhan M. Ahmed, Physical preparation of nanoalloys, in: F. Calvo (Ed.), Nanoalloys From Fundamentals to Emergent Applications, Elsevier, Waltham, 2013, pp. 39–74.
[3] J. Xiao, P. Liu, C. Wang, G. Yang, External field-assisted laser ablation in liquid: an efficient strategy for nanocrystal synthesis and nanostructure assembly, Prog. Mater. Sci. (2017) 140–220.
[4] A. Caricato, A. Luches, M. Martino, Laser fabrication of nanoparticles, in: M. Aliofkhazraei (Ed.), Handbook of Nanoparticles, Springer International Publishing, Switzerland, 2016, pp. 407–428.
[5] N. Semaltianos, Nanoparticles by laser ablation, in: M. Aliofkhazraei (Ed.), Handbook of Nanoparticles, Springer International Publishing, Switzerland, 2010, pp. 67–92.
[6] F. Correard, K. Maximova, M.-A. Estève, C. Villard, M. Roy, A. Al-Kattan, et al., Gold nanoparticles prepared by laser ablation in aqueous biocompatible solutions: assessment of safety and biological identity for nanomedicine applications, Int. J. Nanomedicine 9 (2014) 5415–5430, http://dx.doi.org/10.2147/IJN.S65817.
[7] J. Walter, S. Petersen, F. Stahl, T. Scheper, S. Barcikowski, Laser ablation-based one-step generation and bio-functionalization of gold nanoparticles conjugated with aptamers, J. NanoBiotechnology 8 (2010) 8–21.
[8] Y.-H. Chen, C.-S. Yeh, Laser ablation method: use of surfactants to form the dispersed Ag nanoparticles, Colloids Surf. A. Physochem. Eng. Asp. 197 (2002) 133–139.
[9] J. Bartelmess, S. Giordani, Carbon nano-onions (multi-layer fullerenes): chemistry and applications, Beilstein J. Nanotechnol. 5 (2014) 1980–1998.
[10] D. Mohapatra, S. Badrayyana, S. Parida, Facile wick-and-oil flame synthesis of high-quality hydrophilic onion-like carbon nanoparticles, Mater. Chem. Phys. (2016) 112–119.
[11] M. Zeiger, N. Jäckel, V. Mochalin, V. Presser, Review: carbon onions for electrochemical energy storage, J. Mater. Chem. A 4 (2016) 3172–3196.
[12] H. Zhang, C. Liang, J. Liu, Z. Tian, G. Shao, The formation of onion-like carbon carbon-encapsulated cobalt carbide core/shell nanoparticles by the laser ablation of metallic cobalt in acetone, Carbon 55 (2013) 108–115.
[13] A. De Bonis, A. Santagata, A. Galasso, A. Laurita, R. Teghil, Formation of Titanium Carbide (TiC) and TiC@C core-shell nanostructures by ultra-short laser ablation of titanium carbide and metallic titanium in liquid, J. Colloid Interface Sci. 489 (2017) 76–84.
[14] G. Cristoforetti, E. Pitzalis, R. Spiniello, R. Ishak, F. Giammanco, M. Minuz-Miranda, et al., Physico-chemical properties of Pd nanoparticles produced by Pulsed Laser Ablation in different organic solvents, Appl. Surf. Sci. (2012) 3289–3297.
[15] J.S. Golightly, A.W. Castleman, Analysis of titanium nanoparticles created by laser irradiation under liquid environments, J. Phys. Chem. B 110 (2006) 19979–19984.
[16] A.V. Simakin, V.V. Voronov, N.A. Kirichenko, G.A. Shafeev, Nanoparticles produced by laser ablation of solids in liquid environment, Appl. Phys. A Mater. Sci. Process. 79 (2004) 1127–1132.
[17] V. Amendola, P. Riello, M. Meneghetti, Magnetic nanoparticles of iron carbide, iron oxide, iron@iron oxide, and metal iron synthesized by laser ablation in organic solvents, J. Phys. Chem. C 115 (2011) 5140–5146.
[18] L. Franzel, K. Phumisithikul, M. Bertino, E. Carpenter, Synthesis of multiphasic inhomogeneous Mo/MoC nanoparticles by pulsed laser ablation, J. Nanopart. Res. 15 (2013) 1–6.
[19] A. De Bonis, A. Santagata, M. Sansone, J. Rau, T. Mori, R. Teghil, Femtosecond pulsed laser ablation of molybdenum carbide: nanoparticles and thin film characteristics, Appl. Surf. Sci. (2013) 321–324.
[20] J. Hare, W. Hsu, H. Kroto, A. Lappas, K. Prassides, M. Terrones, et al., Nanoscale encapsulation of molybdenum carbide in carbon clusters, Chem. Mater. (1996) 6–8.
[21] J. Quiroz, E. Frigini Mai, V. Teixeira da Silva, Synthesis of nanostructured molybdenum carbide as catalyst for the hydrogenation of levulinic acid to y-valerolactone, Top. Catal. 59 (2016) 148–158.
[22] X.-H. Wang, H.-L. Hao, M.-H. Zhang, W. Li, K.-Y. Tao, Synthesis and characterization of molybdenum carbides using propane as carbon source, J. Solid State Chem. 179 (2) (2006) 538–543.
[23] Z. Xia, Y. Shen, J. Shen, Z. Li, Mechanosynthesis of molybdenum carbides by milling at room temperature, J. Alloys Compd. 453 (2008) 185–190.
[24] H. Pierson, Handbook of Refractory Carbides & Nitrides: Properties, Characteristics, Processing and Applications, Noyes Publications, New Jersey, 1996.
[25] H. Zhang, J. Liu, Z. Tian, Y. Ye, C. Yunyu, C. Liang, K. Terabe, A general strategy toward transition metal carbide/carbon core/shell nanospheres and their application for supercapacitor electrode, Carbon 100 (2016) 590–599.
[26] H. Kwong, M. Wong, C. Leung, Y. Wong, K. Wong, Formation of core/shell structured cobalt/carbon nanoparticles by pulsed laser ablation in toluene, J. Appl. Phys. 108 (2010) (034304–3).
[27] D. Codorniu, O. Arias, L. Desdín, E. Cazzanelli, L. Caputi, Raman Spectroscopy of polyhedral carbon nano-onions, Appl. Phys. A Mater. Sci. Process. 120 (2015) 1339–1345.
[28] L. Bokobza, J. Brunel, M. Couzi, Raman spectra of carbon-based materials (from graphite to carbon black) and of some silicone composites, Carbon 1 (2015) 77–94.
[29] D. Dorobantu, P. Bota, I. Boerasu, D. Bojin, M. Enachescu, Pulse laser ablation system for carbon NanoOnions fabrication, Surf. Eng. Appl. Electrochem. 50 (2014) 390–394.
[30] J. Du, R. Zhao, Z. Zhu, A facile approach for synthesis and in situ modification of onion-like carbon with molybdenum carbide, Phys. Status. Solid. A 208 (2011)

878–881.
[31] D. Ugarte, Curling and closure of graphitic networks under electron-beam irradiation, Nature 359 (1992) 707–709.
[32] D. Ugarte, Morphology and structure of graphitic soot particles generated in arc-discharge C60 production, Chem. Phys. Lett. 198 (1992) 596–602.
[33] A. Inoue, T. Seto, Y. Otani, Onion-like carbon nanoparticles generated by multiple laser irradiations on laser-ablated particles, Carbon 50 (2012) 1116–1122.
[34] M. Dieterle, G. Weinberg, G. Mestl, Raman spectroscopy of molybdenum oxides. Part I. Structural characterization of oxygen defects in MoO_{3-x} by DR UV/VIS, Raman spectroscopy and X-ray diffraction, Phys. Chem. Chem. Phys. 4 (2002) 812–821.
[35] M. Dieterle, G. Mestl, Raman spectroscopy of molybdenum oxides. Part II. Resonance Raman spectroscopic characterization of the molybdenum oxides Mo_4O_{11} and MoO_2, Phys. Chem. Chem. Phys. 4 (2002) 822–826.
[36] M. Tao, X. Jian, Y. Yong, L. Yongwang, Effect of carburization protocols on molybdenum carbide synthesisand study on its performance in CO hydrogenation, Catal. Today 261 (2016) 101–115.
[37] D. Codorniu Pujals, O. Arias de Fuentes, L. Desdin Garcia, E. Cazzanell, L. Caputi, Raman spectroscopy of polyhedral carbon nano-onions, Appl. Phys. A Mater. Sci. Process. 120 (2015) 1339–1345.
[38] V. Amendola, M. Meneghetti, What controls the composition and the structure of nanomaterials generated by laser ablation in liquid solution, Phys. Chem. Chem. Phys. 15 (2013) 3027–3046.
[39] B. Chicbkov, C. Momma, S. Nolte, F. Alvensleben, A. Tünnermann, Femtosecond, picosecond and nanosecond laser ablation of solids, Appl. Phys. A Mater. Sci. Process. 63 (1996) 109–115.
[40] J. Yoo, S. Jeong, X. Mao, R. Greif, R. Russ, Evidence for phase-explosion and generation of large particles during high power nanosecond laser ablation of silicon, Appl. Phys. Lett. 76 (1999) 783–785.
[41] V. Amendola, M. Meneghetti, Laser ablation synthesis in solution and size manipulation of noble metal nanoparticles, Phys. Chem. Chem. Phys. 11 (2009) 3805–3821.
[42] A. Hassan Hamad, Effects of different laser pulse regimes (nanosecond, picosecond and femtosecond) on the ablation of materials for production of nanoparticles in liquid solution, in: R. Viskup (Ed.), High Energy and Short Pulse Lasers, 2016, pp. 305–325.
[43] R. Intartaglia, K. Bagga, F. Brandi, Study on the productivity of silicon nanoparticles by picosecond laser ablation in water: towards gram per hour yield, Opt. Express 22 (2014) 3117–3127.
[44] J. Tomko, S. O'Malley, C. Trout, J. Naddeo, R. Jimenez, J. Griepenburg, et al., Cavitation bubble dynamics and nanoparticle size distributions in laser ablation in liquids, Colloids Surf. A. Physicochem. Eng. Asp. 522 (2017) 368–372.